

ORIGINAL ARTICLE

Reticence The Effects of Mutagenic Variants in The Xrcc3 Protein: Insights from Computational Drug Discovery and ADMET Properties

U. S. H. Raghavendra Prasad, N. Sravanthi, N. Ravi, M. Kavitha*

Department of Chemistry, University College of Science, Osmania University, Hyderabad 500007, Telangana, India

*Corresponding author's email: kavithamannem@gmail.com; kavithamannem@osmania.ac.in

ABSTRACT

XRCC3 (X-ray repair cross-complementing protein 3) is a critical human protein functions in maintaining genomic integrity by repairing DNA. Specifically, within the homologous recombination repair (HRR) pathway, this is vital for fixing double-strand breaks in DNA. Mutations in XRCC3 can hinder this repair process, potentially cause genomic instability and increase the risk of cancer development. In XRCC3 protein T241M (Threonine to Methionine at position 241) polymorphism is a prevalent genetic variation linked to a higher susceptibility to several cancers. Functional studies indicate that this mutation might impair DNA repair efficiency, particularly in homologous recombination repair, potentially resulting in increased genomic instability and greater vulnerability to mutations during cell division. Consequently, this may reduce the proteins effectiveness in repairing DNA double-strand breaks. In this probe, we are leveraging sophisticated computational algorithms to precisely target XRCC3 mutations and elucidate potential inhibitory molecules.

Keywords: XRCC3 (X-ray repair Cross-Complementing protein 3), HRR (Homologous Recombination Repair), DNA double strand break, Computational algorithm

Received 20.03.2025

Revised 12.05.2025

Accepted 29.05.2025

How to cite this article:

U. S. H. Raghavendra Prasad, N. Sravanthi, N. Ravi, M. Kavitha. Reticence The Effects of Mutagenic Variants in The Xrcc3 Protein: Insights from Computational Drug Discovery and ADMET Properties. Adv. Biores., Vol 16 (3) May 2025: 196-206.

INTRODUCTION

Breast cancer continues to be a dominant and serious health concern for women around the world. It arises from the uncontrolled growth of cells within the breast tissue and can vary widely in terms of molecular subtype, aggressiveness, and response to treatment. In recent years, its incidence has increased significantly have improved survival rates, the underlying causes of breast cancer remain complex and multifunctional-encompassing genetic, hormonal, environmental, and lifestyle- related factors. Ongoing research continues to explore the biological mechanisms of tumor development and progression, aiming to enhance prevention strategies, diagnostic accuracy, and personalized treatments.

Genetic variation and environmental factors together contribute to cancer development. DNA repair genes play a key role in maintain genomic stability by fixing damage from sources like UV radiation or internal mutagens [10-12]. Faulty repair of double-strand breaks (DSBs) leads to genome instability, a key feature of cancer [13]. Double strand Breaks are fixed by twofold pathways: Homologous DNA recombination (HDR) and non - homologous end joining (NHEJ) [14,15]. In breast cancer cell, HR activity is elevated, while NHEJ remains the primary repair route in both normal and cancerous cells, with similar efficiency. RAD51 family [16,17], a critical protein family in HR, is essential for accurate DNA repair and genome maintenance.

Biochemical Pathway

XRCC3 (X-ray repair cross-complementing protein 3) is a member of the RAD51 paralog family [18], which plays crucial role in the homologous recombination (HR) pathway of DNA double-strand break repair (Figure 1) [1,2]. When a DNA break occurs, HR is activated during the S and G2 phases of the cell

cycle, where a sister chromatid is available as a template. The process begins with DNA end resection, producing single-stranded DNA overhangs. These overhangs are coated with replication protein A (RPA), which is later replaced by RAD51, assisted by XRCC3 and other paralogs. XRCC3 stabilizes the RAD51 nucleoprotein filament, promoting strand invasion and homology search. This leads to the formation of a displacement loop (D-loop), allowing DNA synthesis to restore the damaged region using the sister chromatid as a guide [3-9].

In breast cancer, XRCC3 plays a dual role [19]. On one hand, its function in maintaining genome stability protects cell from malignant transformation on the other hand dysregulation or polymorphism in XRCC3 can compromise DNA repair efficiency, leading to the accumulation of mutations and promoting tumor progression. Overexpression or altered activity of XRCC3 has been observed in breast cancer subtypes, potentially contributing to resistance against DNA-damaging therapies. Thus, XRCC3 serves not only as a guardian of genomic integrity but also as a potential biomarker for cancer susceptibility and treatment response.

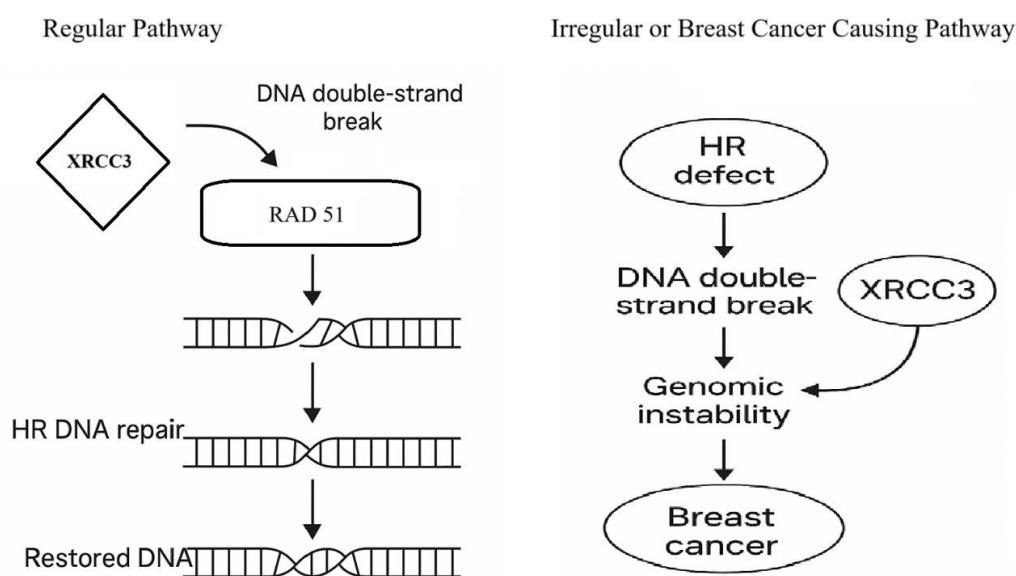


Figure 1. XRCC3 Protein Regular and Irregular Pathway

MATERIAL AND METHODS

In recent years, computational chemistry techniques have been increasingly utilized to address the shortcomings of conventional drug discovery approaches. To date, a completely resolved three-dimensional (3D) structure of the XRCC3 protein has not been determined through either experimental analysis or theoretical modelling. Therefore, the present study focuses on constructing and validating a 3D structural model of XRCC3 using *in silico* approaches [20]. The amino acid sequence of XRCC3 in FASTA format was obtained from the Universal Protein Resource (UniProt) [21]. Proteins exhibiting similar secondary structures, domain arrangements, and folding patterns were selected as templates using the Jpred4, and PHYRE2 tools, respectively [21-23]. The degree of sequence-to-structure conservation between XRCC3 and templates is quantitatively assessed using the statistical metric known as the E-value.

Protein sequence alignment and 3D model construction

The amino acid sequence of the target protein was aligned with template sequences through CLUSTALW [24]. A three-dimensional structure of the XRCC3 protein was then constructed using MODELLER, which employs the CHARMM22 force field [25]. The model exhibiting the lowest objective function score from MODELLER was chosen for subsequent optimization studies.

Energy minimization and Validation

The quality of the generated 3D protein model was refined through loop modeling and energy minimization was conducted with the Impref Module from the Schrodinger suite [26], employing a cutoff of 0.3 Å. This process utilized the OPLS 2004 (Optimized Potential for Liquid Simulation) force field [27], which helps preserve the protein's native carbon backbone structure. During this step, the backbone atoms were kept fixed while side chains were allowed to adjust, enabling the structure to reach a low-energy conformation without altering the C α atom coordinates.

To further enhance model stability, molecular dynamics simulations were performed using the Protein Preparation Wizard in the Schrodinger Suite applied the OPLS-AA force field (all-atom variant) to optimize the 3D structural quality [28].

The structural integrity and validity of the homology model was assessed using PROCHECK [29], ProSA [30], and VERIFY_3D servers [31]. Root means square deviation (RMSD) analysis was conducted between the template structure and the target protein to evaluate the accuracy of the homology model for XRCC3. The conformation exhibiting the highest stability was selected for further examination, including its secondary structure elements and potential active site regions.

Active site identification by computational approach

Accurate identification of a protein's active site is fundamental for elucidating its precise biological role and plays a critical role in rational drug design and discovery. Advanced computational approaches are utilized to predict potential ligand-binding pockets within the protein structure. Tools such as CASTp and the SiteMap module within the Schrodinger suite are employed to detect hydrophobic cavities and topologically favorable binding regions [28,32,33].

Virtual Screening and Molecular Docking

A receptor grid was generated at the predicted binding domain of the XRCC3 protein using the Glide Module from the Schrodinger suite to facilitate virtual screening and molecular docking analyses. Ligand molecules were curated from established structural databases and prepared for docking using LigPrep, which optimizes their stereochemistry, ionization states, and ring conformations to ensure accurate binding predictions [33]. The virtual screening workflow in Glide was executed sequentially using HTVS (High Throughput Virtual Screening), SP (Standard Precision), and XP (Extra Precision) docking protocols. Docked ligands were subsequently ranked based on their Glide Scores [34,35,36], which reflect predicted binding affinity.

ADMET Properties

Comprehensive evaluation of Absorption, Distribution, Metabolism, Excretion, and Toxicity (ADMET) properties is an essential component of early-phase drug development, influencing both clinical trial viability and eventual market success of lead compounds. Ligand molecules identified through virtual screening and docking-particularly those demonstrating significant binding affinity toward XRCC3 were subjected to ADME profiling using the QikProp module within the Schrodinger suite. To further assess toxicity and synthetic accessibility, Pro Tox 3.0 web platform was employed [37-40]. Ligands exhibiting favorable ADME and toxicity profiles were shortlisted as promising therapeutic candidates for Breast cancer.

RESULTS AND DISCUSSION

Three-dimensional conformational assessment of the XRCC3 protein

Acquisition of the amino acid sequence data and identification of structural template

The UniProt server, an integral resource in bioinformatics, provides a curated protein sequence and annotation database that supports a wide range of biological research. It combines data from Swiss-Prot, TrEMBL, and PIR Databases, offering comprehensive information on protein sequences, functional annotations, structural features, and taxonomy. UniProt simplifies protein searches by enabling query-based retrieval and provides downloadable FASTA sequences essential for downstream analysis.

In this study, the UniProt server [21] was employed to retrieve protein sequences for XRCC3 Protein, which were further analyzed for functional annotations and structural insights. These sequences were critical in identifying conserved regions and active sites for homology modeling. By using accession numbers or sequence based queries, the server ensured accurate and reproducible data, contributing significantly to our computational workflow.

Template Selection

The BLAST (Basic Local Alignment Search Tool) server was employed to identify a suitable structural template for XRCC3, a protein involved in DNA repairing pathway. Using the BLASTP algorithm, the search prioritized templates with high sequence identity, low E-value (< 0.001), and significant query coverage to ensure structural accuracy and evolutionary relevance. Among the results, the template 8FAZ_B was selected as it exhibited strong homology to XRCC3 protein. This selected template served as the foundation for subsequent 3D modeling and structural analysis, highlighting the BLAST server's utility in homology-based structural predictions.

Table 1: Template selection of XRCC3 Protein

S. NO.	Template Search Tool	Template identified	% Identity	E-value/ % Confidence
1	PSI- BLAST	8FAZ_B	29.14	2×e-22
2	Jpred4	8FAZ_B	82.00	5×e-21
3	PHYRE2	8FAZ_B	29.00	100%

The Jpred4 tool detects template proteins that share similar secondary structures by utilizing multiple sequence alignment profiles. It applies the JNet algorithm to predict the most likely secondary structure components of proteins, including α -helices, β -sheets, and loops.

To predict the 3D structure of the target protein, the amino acid sequence in FASTA format submitted to the Phyre2 web server (Kelley et al., 2015). The sequence was analyzed using Hidden Markov Model (HMM) - based alignment, comparing it with structural templates in the Protein Data Bank (PDB). Template selection was based on sequence identity, coverage, and confidence score. After selecting the best structural template, homology modelling was performed to generate a predicted 3D structure of the protein.

Sequence alignment and Structural Validation of XRCC3 protein

The XRCC3 protein sequence was reliably aligned with evolutionarily related template protein sequences, providing a strong foundation for constructing an accurate 3D structure. The FASTA sequence of XRCC3, along with the chosen template 8FAZ_B and their atomic coordinates (FIGURE 2), was input into MODELLER to build its three-dimensional model. A total of 50 models were generated, and the one with the lowest objective function value was selected for further refinement and optimization studies.

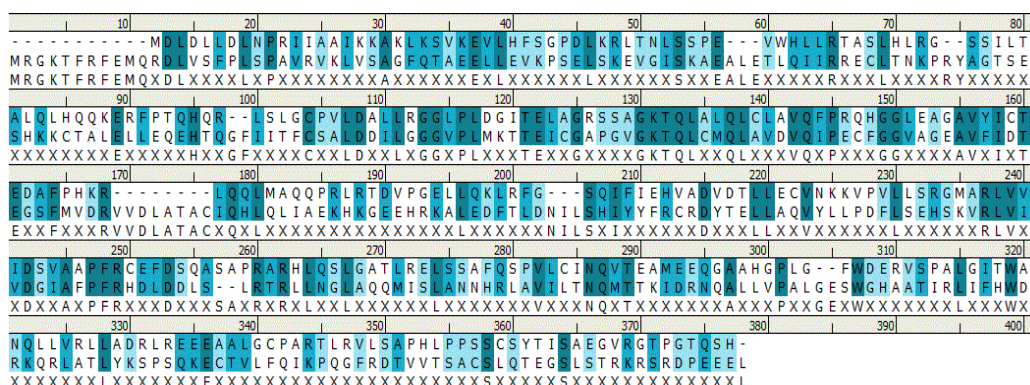


Figure 2. Alignment of XRCC3 protein with template sequence 8FAZ_B

Figure 2 shows the sequence alignment of the XRCC3 protein with its template 8FAZ_B sequence, which was CLUSTALW and visualized through Discovery Studio v24.1.0. In the alignment visualization, conserved residues are highlighted in dark green, strongly similar residues in light blue, and weakly similar residues in white, illustrating the degree of evolutionary conservation across the aligned sequence.

The generated 3D model was further refined using structural validation tools such as ProSA and Verify 3D. The predicted structure is valuable for protein ligand-docking, functional studies, and discovery applications.

Model Validation

The stereo chemical integrity of the XRCC3 protein model was evaluated using the Ramachandran plot (Figure 3) [41] [42] [43], which revealed that 90.0% of the residues reside within energetically favorable regions. Structural validation of amino acid compatibility in the three-dimensional model was conducted using the VERIFY_3D tool [37], which assesses the correlation between the 1D amino acid sequence and its 3D environment. Results indicated that 90.0% of the 346 residues achieved a 3D-1D score exceeding 0.2, confirming acceptable model quality. Further evaluation using the ProSA-web server [37] (Figure 4 and 5) supported the structural reliability by benchmarking the model against proteins of similar size in the Protein Data Bank (PDB), assessing both global and local quality.

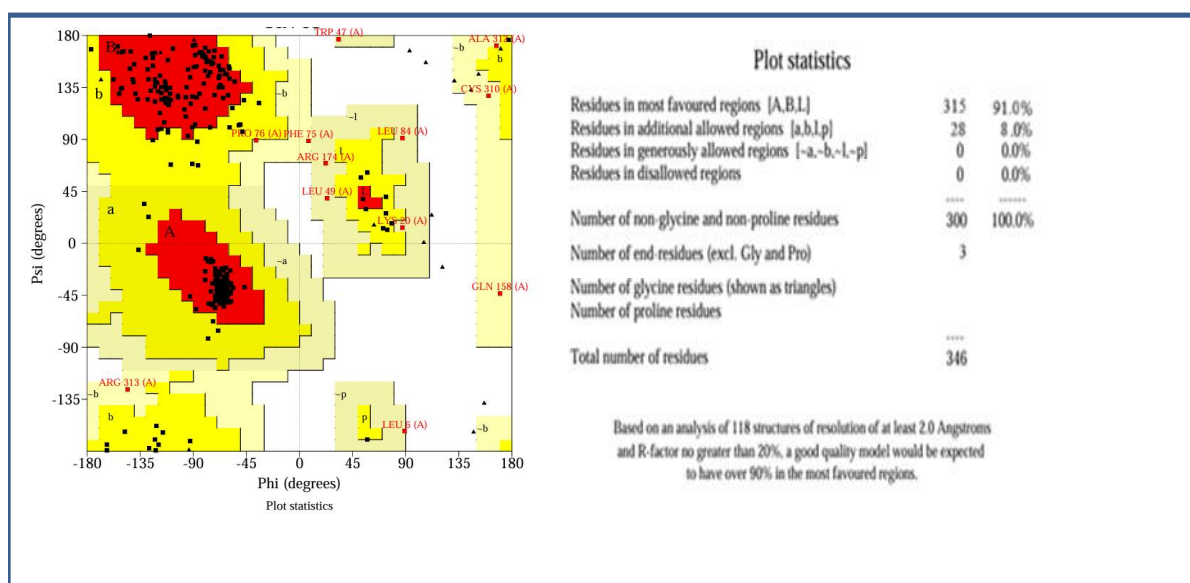


Figure 3: Ramachandran contour plot of the XRCC3 protein structure to assess the stereochemical quality

The Ramachandran plot illustrated in Figure 3 indicates that approximately 91% of the XRCC3 protein residues occupy energetically favorable regions. The high percentage suggests excellent stereo chemical quality. Protein models exhibiting over 90% of residues within the most favored regions are generally considered structurally stable.

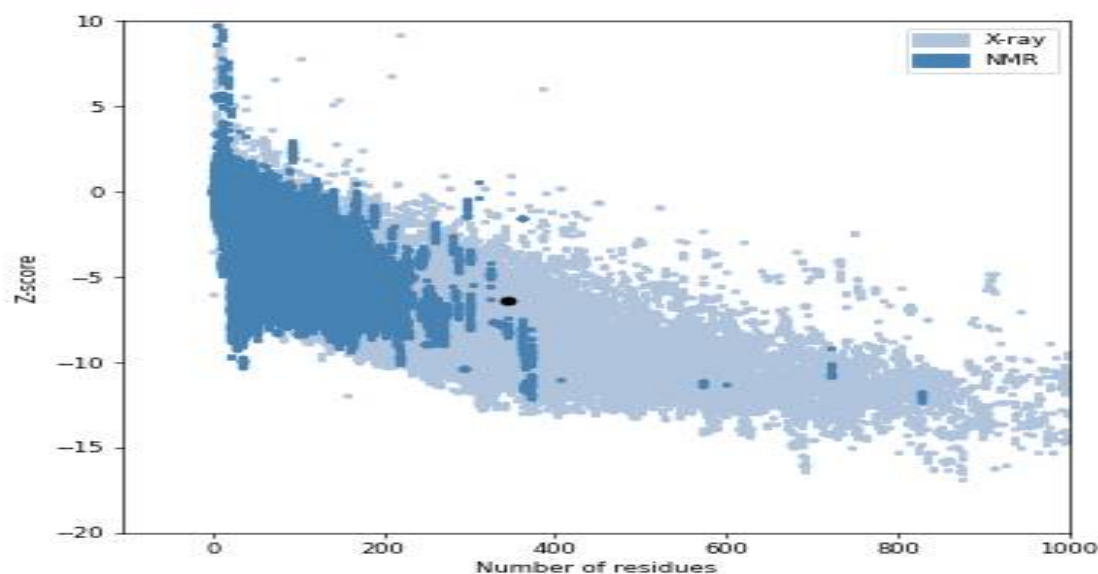


Figure 4: Overall model quality assessment of the XRCC3 protein

Figure 4 presents the ProSA evaluation graph for the XRCC3 protein model, highlighting its Z-score, which serves as a measure for assessing the structural integrity of the predicted model. The obtained Z-score of -6.39 falls within the range typically observed for native protein structures of comparable size in the Protein Data Bank (PDB), thereby indicating a high degree of reliability and similarity in terms of overall 3D structural quality.

The overall Z-score of the XRCC3 protein model, calculated as -6.39 (Figure 4) falls within the acceptable range observed for experimentally determined structures of comparable size resolved by X-ray crystallography (light blue) and NMR spectroscopy (dark blue). This score reflects a high-quality model with structural integrity. Additionally, the ProSA energy plot (Figure 5) evaluates the local structural quality using knowledge-based energy calculations, illustrating energy variations across the sequence.

with two smoothing window size (10 and 40 residues), highlighting regions of potential instability or deviation [37].

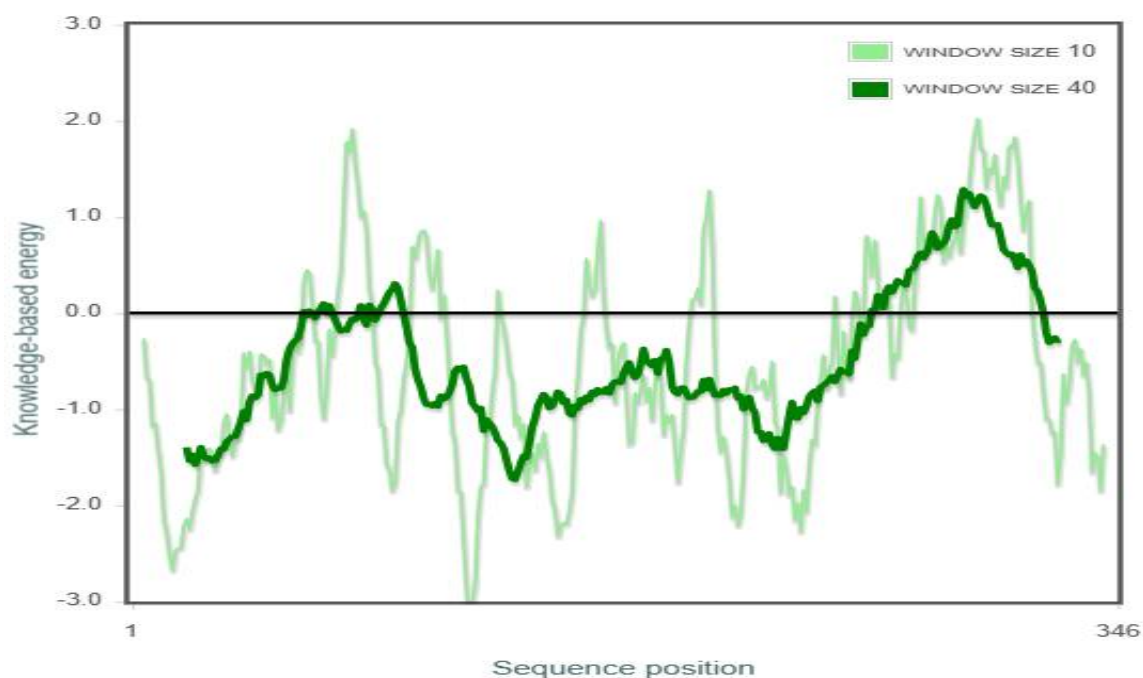


Figure 5: Local model quality assessment of the XRCC3 protein

Figure 5 illustrates the local quality assessment of the XRCC3 protein structure, based on a knowledge-based energy profile. The energy plot evaluates individual amino acid residues using two window sizes-10 residues (light green) and 40 residues (dark green). The majority of the energy values lie below the baseline, indicating a favorable local structural quality and suggesting that most region of the protein adopt energetically stable conformations. Figure 6 shows the ribbon model of the XRCC3 protein comprising of 17 α helices, 15 β sheets and 3 β hairpins.



Figure 6: Computationally modeled XRCC3 protein structure

e) Structural profiling of alpha-helices and beta-sheets

The 3D model of the XRCC3 protein is composed of 17 α helices, 15 β sheets and 3 β hairpins. (Figures 6 and 7).

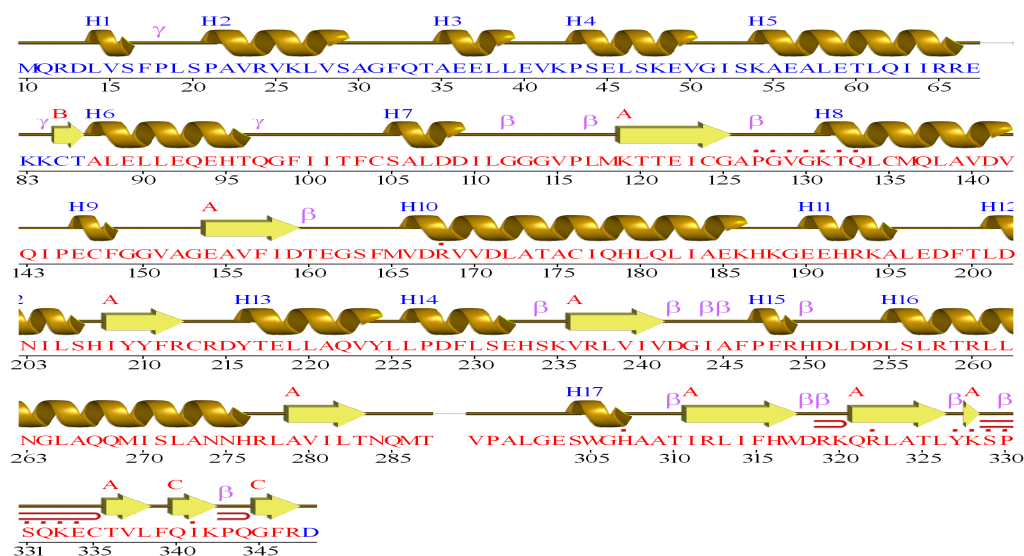


Figure 7: Analysis of the secondary structure of XRCC3 protein

Figure 7 presents a schematic representation of the secondary structural elements of the XRCC3 protein, generated using the PDB-Sum server [44,45]. The diagram outlines the arrangement of secondary structures (α helices and β sheets).

Identification of XRCC3 protein active site through computational method

To identify potential ligand-binding regions, computational tools such as CASTp and SiteMap were employed. CASTp analyzes topographical features of proteins by incorporating Connolly's molecular surface and Richards' solvent-accessible surface models. As shown in Table 2, suggesting possible functional or ligand-interaction sites within this segment of the XRCC3 structure.

Table 2: The potential active site residues of XRCC3

S. NO.	Active site prediction tool / server	Site number	Amino acids	Volume of the site (Å)
1	SiteMap	1	6,7,8,10,13, 55,58,59,60,61, 63,68,69,71,72, 73,78,80,93,94, 98,99,100,101, 102,232,233,235, 236,239,240,243, 246,247,284,285, 286,287,288,290, 291,293,294,320, 321,322,323	548.8
		2	9,10,11,44,45,51, 191,195,196,199,200, 237,238,240,241,244	253.134
2	CASTp	1	105,109,220,223, 225,226,227,228, 231,232,258,259, 260,261,262,263, 265,267,269,270, 271,275,277,279, 284,285,300	670.094
		2	108,109,220,223, 225,226,227,228, 231,232,258,259, 260,261,262,263, 264,265,267,269, 270,271,272,275, 276,277,279,283, 284,285,300	438.577

CASTp analysis identified two larger binding pockets, whereas SiteMap revealed comparatively similar hydrophobic regions. The CASTp – derived sites and SiteMap findings in agreement with protein-protein interactions (PPI) studies, suggest that this region serves as the functional active site of XRCC3 protein.

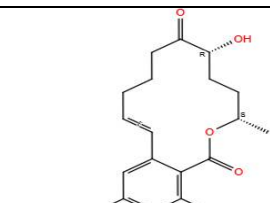
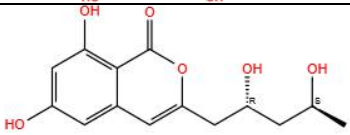
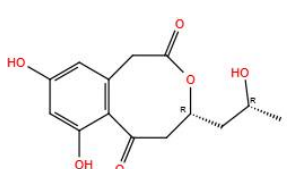
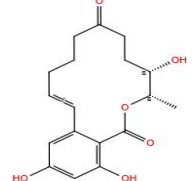
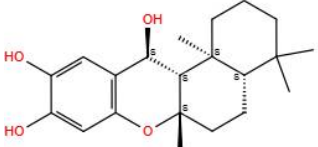
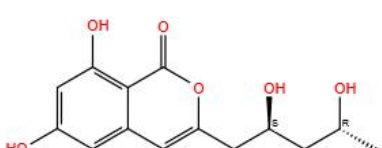
Structure-based virtual screening and docking studies

In this study, structure-based virtual screening (SBVS) was employed to discover novel ligand candidates targeting the XRCC3 protein. A grid of $64 \text{ \AA} \times 64 \text{ \AA} \times 64 \text{ \AA}$ was defined at the protein's active site to facilitate docking. Ligands were pre-processed using Schrodinger's LigPrep Module (LigPrep, version 2023, Schrödinger, LLC, New York, NY, 2023) which optimized molecular geometry, generated energetically favorable conformers, and produced various ionization and tautomeric states using Epik. Adjustments were made to ensure stereochemical and structural integrity, especially in fused ring systems.

30,000 molecules from the Comprehensive Marine Natural Products Database (CMNPD) were subjected to LigPrep and 45,619 ligand structures were generated as an output 46-48. These were subjected to hierarchical docking using HTVS, SP, XP protocols in Glide (Glide, version, Schrödinger, LLC, New York, NY, 2023), progressively narrowing candidates based on binding affinity. From this screening, 25 ligands showed promising interactions, and top ten representative ligand-protein complexes were ranked by Glide score (Table 3, Figure 8).

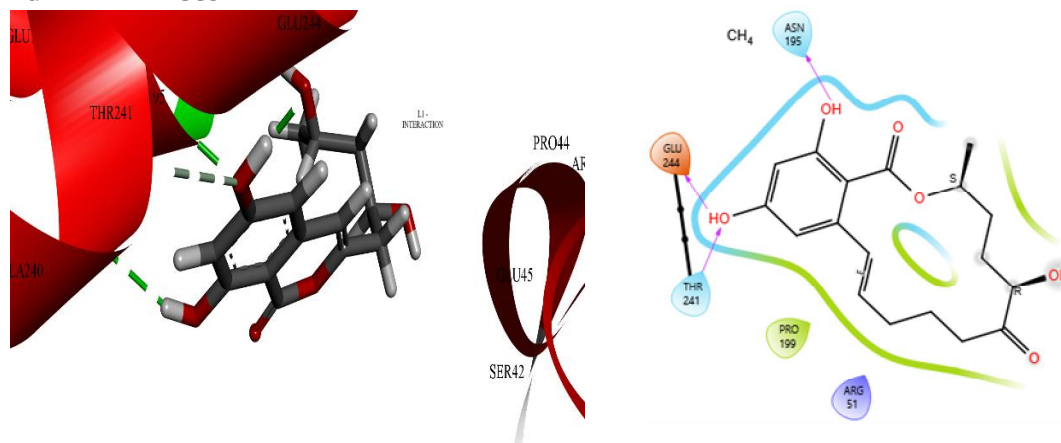
Analysis revealed favorable hydrogen bonding interactions, with bond lengths ranging from 1.48 \AA to 2.68 \AA (Table 4). These interactions were visualized in Accelrys Discovery Studio Visualizer v24.1.0 (49), supporting the ligands' potential for strong XRCC3 binding.

Table 3: Docking glide score and glide energy

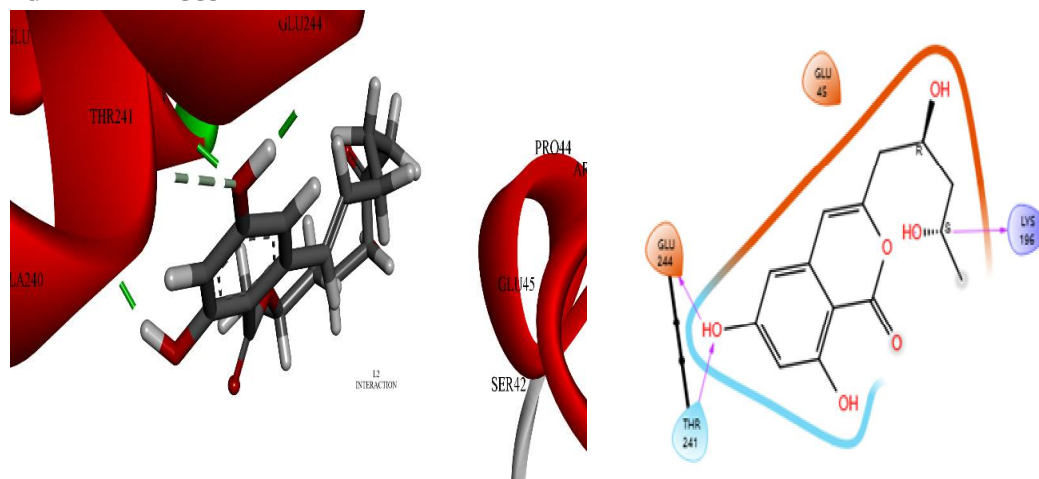
Serial Number	Ligand structure	Glide energy(kcal/mol)	Glide Score	H- Bond Interactions	H - Bond Distance (Å)
L1		-42.603	-7.250	L1- ARG 51 L1- THR 241 L1- ASN 195	1.50 1.87 1.73
L2		-39.835	-7.215	L2- ASN 195 L2- THR 241 L2- LYS 196 L2- GLU 244	2.06 1.93 1.62 1.61
L3		-40.616	-7.320	L3- THR 241 L3- GLU 244 L3- LYS 196 L3- ASN 195	1.86 1.48 2.00 1.89
L4		-45.057	-7.144	L4- ASN 195 L4- THR 241 L4- GLU 244	1.76 1.95 1.68
L5		-42.350	-7.101	L5- THR 241 L5- GLU 244 L5- LYS 196 L5- ASN 195	1.98 1.57 2.00 1.94
L6		-45.459	-6.968	L6- ASN 195 L6- THR 241 L6- GLU 244 L6- ASN 9	1.58 2.11 1.73 2.68

The table 3 presents representative ligand structures and their binding profiles with the XRCC3 protein, selected from 25 docked complexes through virtual screening using the comprehensive marine natural products database. Glide docking scores, interaction energies, and hydrogen bonding data are included. Most ligands consistently interact with key XRCC3 residues ASN-195, LYS-196, THR-241, GLU-244 highlighting their specificity and favorable binding affinity. Notably, ligands featuring M1 to M6 emerged as pharmacophores with potential inhibitory activity against XRCC3 protein.

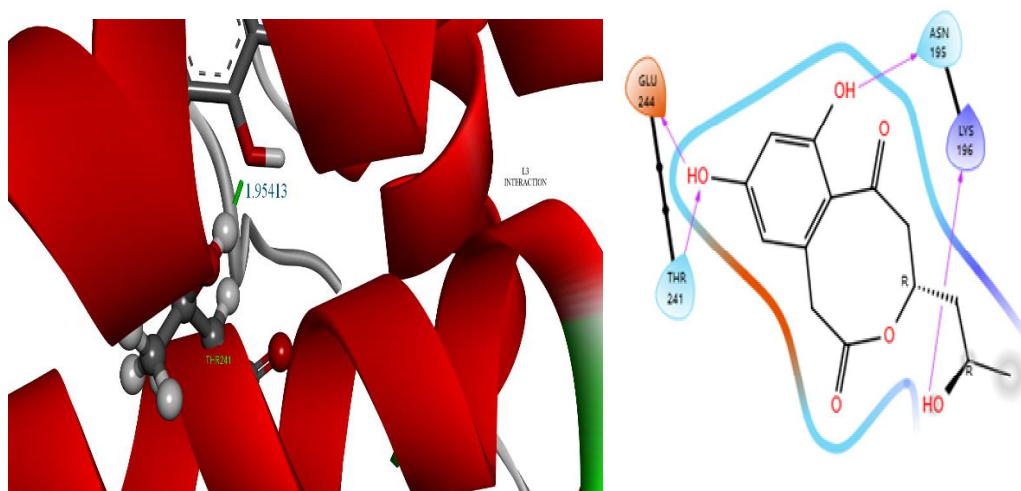
LIGAND 1 – XRCC3



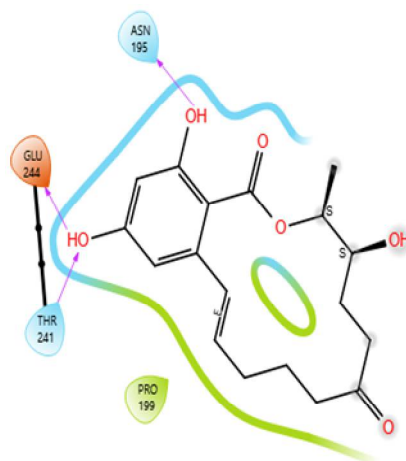
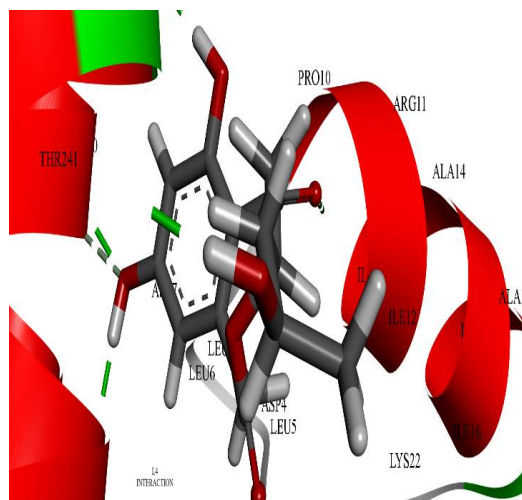
LIGAND 2 – XRCC3



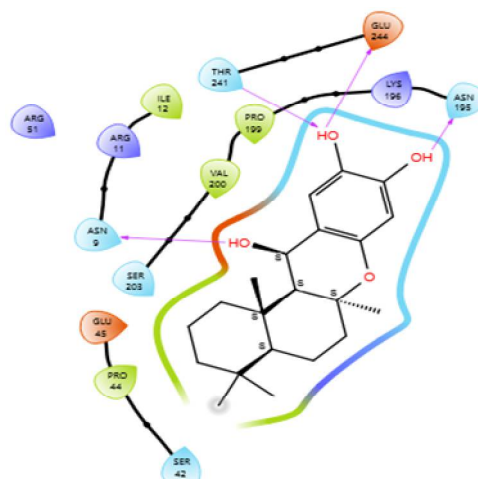
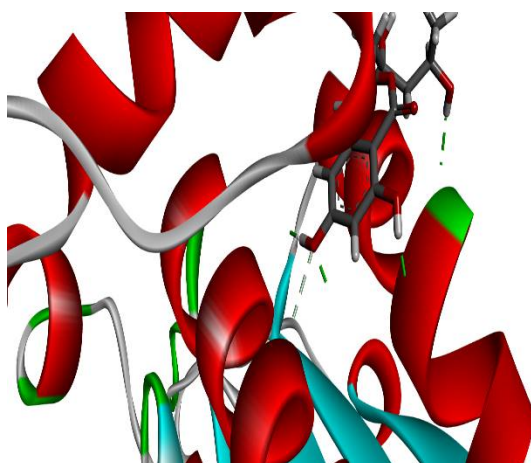
LIGAND 3 – XRCC3



LIGAND 4 – XRCC3



LIGAND 5 - XRCC3



LIGAND 6 – XRCC3

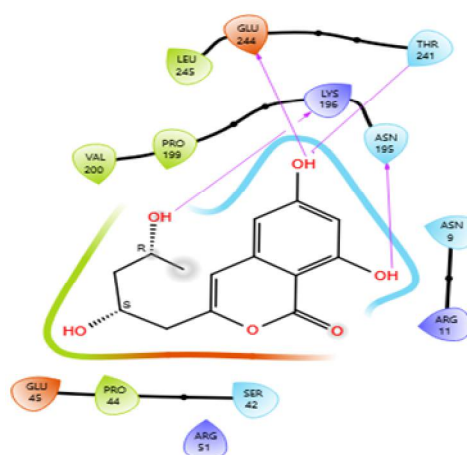
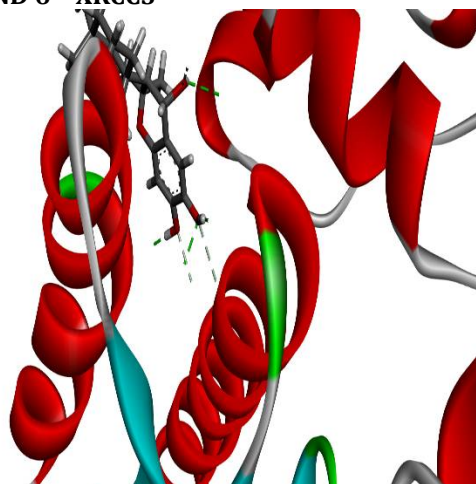


Figure 8: Interpretation of interactions between ligand and XRCC3 protein using Accelrys Discovery Studio Visualizer v24.1.0 and Schrödinger Suite

ADMET (Absorption Distribution Metabolism Elimination and Toxicity)

Physicochemical Properties

Evaluation of ADME (Absorption, Distribution, Metabolism, and Excretion) properties is a crucial step in the early stages of drug development [24]. In this study, the pharmacokinetic profiles of the lead compounds and existing XRCC3 – interacting drugs were assessed using the QikProp module from the Schrödinger suite (refer to table 4 and 5). The analysis included physiochemical parameters such as

molecular weight (≤ 384.1), and hydrogen bond donor and acceptor values, which fell within acceptable limits (donors ≤ 5 ; acceptors ≤ 9.5), supporting their drug-likeness.

Pharmacokinetic properties

Human oral absorption (HOA) is a key parameter in early drug development. The evaluated ligands demonstrated favorable HOA percentages, ranging from 61.474% to 94.049%, indicating strong potential for oral bioavailability. The solubility of a compound, crucial for its systemic uptake, was assessed through QPlogS values, which remained within the acceptable range (-2.093 to -4.573). Intestinal permeability, indicated by QPPCaco values, also fell within permissible levels (59.525- 525.233), suggesting efficient gut absorption.

To evaluate plasma protein binding, QPlogKhsa values were examined, showing appropriate binding affinities (-0.511 to 0.503). As blood –barrier (BBB) permeability affects central nervous system (CNS) toxicity, QPlogBB values were also considered and found to lie between -1.955 to -0.782, suggesting limited CNS penetration. Moreover, CNS activity scores for the ligands were negative, indicating minimal neurotoxicity risk. Lastly, potential cardiac toxicity was assessed using predicted hERG channel inhibition (pIC50). All ligands showed acceptable inhibitory values from -3.807 to -4.118 (figure 4 and 5).

Table 4: Predicted pharmacokinetic and drug likeness properties of identified ligands obtained from virtual screening

Ligand Number	Physicochemical Properties				Pharmacokinetic properties							Drug Likeness Property		
	mol_MW	donorHB	acceptorHB	QPlogS	HOAs%	QPPCaco	QPlogKhsa	QPlogPw	QPlogBB	CNS	QPlogHERG	Rule Of Five	Rule Of Three	QPlogPo/w
L1	334.368	2	6.2	-3.92	71.79	90.378	0.114	11.569	-1.503	-2	-4.062	0	0	1.68
L2	280.277	3	6.4	-2.093	61.474	60.923	-0.511	12.217	-1.947	-2	-4.088	0	0	0.441
L3	280.277	2	7.2	-2.33	61.834	70.425	-0.475	11.947	-1.671	-2	-3.807	0	0	0.311
L4	334.368	2	6.2	-3.82	72.52	98.472	0.108	11.555	-1.443	-2	-3.981	0	0	1.69
L5	280.277	3	6.4	-2.095	61.355	59.525	-0.508	12.275	-1.955	-2	-4.118	0	0	0.449
L6	346.466	3	3.95	-4.573	94.049	525.233	0.503	10.178	-0.782	-1	-3.888	0	0	3.145

Table 5: Permissible ranges of Absorption Distribution Metabolism Elimination

S. No.	Descriptor	ADME Property	Permissible Ranges or Recommended Value
1	CNS	Predicted central nervous system activity on -2 to +2 scale	-2 (inactive) to +2 (active)
2	mol_MW	Molecular weight of the molecule	130 to 725
3	DHB	Estimated number of hydrogen bonds donated by solute in aqueous solution	0 to 6
4	AHB	Estimated number of hydrogen bonds accepted by solute in aqueous solution	2 to 20
5	QPPCaco	Predicted Caco-2 cell permeability (nm/sec)	<25 = poor, >500 = great
6	QPlogPw	Predicted water/gas partition coefficient	4.0 – 45.0
7	QPlogPo/w	Predicted octanol/water partition coefficient	-2.0 – 6.5
8	QPlogS	Predicted aqueous solubility, log S (mol/dm ³)	-6.5 – 0.5
9	QPlogKhsa	Predicted binding to human serum albumin	-1.5 – 1.5
10	QPlogHERG	Predicted IC ₅₀ for blockage of HERG K ⁺ channels	Below +5.0
11	QPlogBB	Predicted blood/brain partition coefficient	-3.0 – 1.2
12	% Human Oral Absorption	Predicted human oral absorption on 0 to 100% scale	>80% = high; <25% = poor
13	Rule Of Five	Number of violations of Lipinski's Rule of Five	Maximum is 4
14	Rule Of Three	Number of violations of Jorgensen's Rule of Three	Maximum is 3
15	Synthetic Feasibility	Predicted synthetic feasibility on scale of 1 to 10	0 = high feasibility, 10 = least feasible
16	Lipophilicity	Predicted lipophilic nature (pIC50 – LogP)	min -6; max +3

Drug likeness properties

All selected ligands comply with Lipinski's rule of five and Jorgensen's rule of three [50] [51], indicating favorable drug-like properties. Their lipophilicity, which influences membrane permeability and transport, is within an acceptable range, with QPlogPo/w values spanning from 0.311 to 3.145 (Table 5). These results reflect satisfactory ADME profiles.

Toxicity

A significant number of therapeutic agents undergo metabolism via the cytochrome P450 (CYP450) enzyme system. Any disruption in these pathways may result in toxic outcomes. To assess the potential toxicity of the identified ligands, the Pro Tox 3.0 tool was utilized (Table 6). The impact of the ligands on the CYP450 enzymes was evaluated to determine whether they act as inhibitor (+) or non-inhibitor (-). This modulatory behavior is essential for dose optimization and possible drug combination and possible drug combinations. The ADMET analysis [53] indicates that the screened ligands exhibit improved drug-like characteristics and synthetic accessibility compared to conventional drugs, suggesting their potential as novel candidates for Breast Cancer.

Table 6: Predicted toxicity using ProTox-3.0 server

S. NO.	CYP1A2	CYP2C19	CYP2C9	CYP2D6	CYP3A4
L1	INACTIVE	INACTIVE	INACTIVE	INACTIVE	ACTIVE
L2	INACTIVE	INACTIVE	INACTIVE	INACTIVE	INACTIVE
L3	INACTIVE	INACTIVE	INACTIVE	INACTIVE	INACTIVE
L4	INACTIVE	INACTIVE	INACTIVE	INACTIVE	INACTIVE
L5	INACTIVE	INACTIVE	INACTIVE	INACTIVE	INACTIVE
L6	INACTIVE	INACTIVE	INACTIVE	INACTIVE	ACTIVE

Table 6 displays the potential toxic effects of ligand L1 to L6 on the Cytochrome p450 enzyme. It outlines whether each ligand and the breast cancer drug act as inhibitors (indicated by positive values) or non – inhibitors (indicated by negative values) of the p450 enzyme system.

The identified ligands, exhibit both positive and negative inhibition values, suggesting a low likelihood of causing adverse interactions. According to the predicted ADMET results, the ligands (L1 TO L6) obtained through virtual screening demonstrate more favorable drug-likeness characteristics. Therefore, these compounds hold potential as promising candidate for developing new breast cancer inhibitors.

CONCLUSION

The present study effectively elucidates the structural and functional insights of the XRCC3 protein, a critical player in homologous recombination-mediated DNA repair, and highlights its role in breast cancer pathogenesis. By constructing a high-fidelity three-dimensional model of XRCC3 using computational homology modeling tools, key structural features and potential active sites were identified with confidence. Structure-based virtual screening of marine natural product libraries enabled the selection of six promising ligands (L1–L6) based on strong binding affinities and stable protein-ligand interactions at critical residues such as THR241, ASN195, GLU244, and LYS196. The identified ligands were further validated through detailed ADMET profiling, revealing excellent pharmacokinetic and drug-likeness properties, including favorable molecular weights, solubility, permeability, oral absorption, and low CNS activity, with no violations of Lipinski's Rule of Five or Jorgensen's Rule of Three. Moreover, toxicity analysis using the ProTox 3.0 platform confirmed the non-toxic behavior of these ligands, with minimal inhibitory effects on key cytochrome P450 enzymes, indicating reduced risk of drug-drug interactions and metabolic complications. Notably, all ligands displayed low hERG inhibition values, minimizing potential cardiotoxicity. Among them, Ligand L6 exhibited superior Caco-2 permeability and oral absorption, suggesting excellent bioavailability. Collectively, the integration of molecular modeling, docking, ADMET evaluation, and toxicity assessment offers a comprehensive framework for early-phase drug discovery. In summary, this study identifies potent and selective XRCC3 inhibitors with drug-like characteristics, which could serve as promising therapeutic candidates for breast cancer intervention. The findings not only reinforce the therapeutic potential of targeting XRCC3 in cancer therapy but also exemplify the power of in silico methods in accelerating drug discovery pipelines. Further in vitro and in vivo studies are warranted to validate these compounds' efficacy and safety.

REFERENCES

1. Pant, P. R., & Yu, J. (2023). Relationship between polymorphisms in homologous recombination repair genes RAD51 G172T, XRCC2 & XRCC3 and risk of breast cancer: a meta-analysis. *Frontiers in Oncology*, 13, 1047336.
2. Chai, F., Liang, Y., Chen, L., Zhang, F., & Jiang, J. (2015). Association between XRCC3 Thr241Met polymorphism and risk of breast cancer: meta-analysis of 23 case-control studies. *Medical Science Monitor*, 21, 3231–3240.

3. He, J., & Xu, J. (2019). XRCC3 Thr241Met polymorphism and breast cancer risk: A meta-analysis of 55 studies. *Medicine*, 98(31), e16592.
4. Kuschel, B., et al. (2002). A population-based breast cancer case-control study identifying XRCC3 T241M association with increased breast cancer risk. *Cancer Epidemiology, Biomarkers & Prevention*, 13(4), 583–589.
5. Figueiredo, J. C., et al. (2004). Polymorphisms XRCC1-R399Q and XRCC3-T241M and the risk of breast cancer at the Ontario site of the Breast Cancer Family Registry. *Cancer Epidemiology, Biomarkers & Prevention*, 13(4), 583–589.
6. Mao, C.-F., Qian, W.-Y., Wu, J.-Z., Sun, D.-W., & Tang, J.-H. (2014). Association between the XRCC3 Thr241Met polymorphism and breast cancer risk: an updated meta-analysis of 36 case-control studies. *Asian Pacific Journal of Cancer Prevention*, 15(16), 6613–6618
7. Economopoulos, K. P., & Sargentanis, T. N. (2010). XRCC3 Thr241Met polymorphism and breast cancer risk: a meta-analysis. *Breast Cancer Research and Treatment*, 121(2), 439–444
8. Manuguerra, M., Saletta, F., Karagas, M. R., Berwick, M., Veglia, F., Vineis, P., & Matullo, G. (2006). XRCC3 and RAD51 polymorphisms as modulators of cancer susceptibility: a meta-analysis. *Journal of the National Cancer Institute*, 98(1), 41–54.
9. Sobczuk A, Romanowicz-Makowska H, Fiks T, Baszczyński J, Smolarz B. (2009). XRCC1 and XRCC3 DNA repair gene polymorphisms in breast cancer women from the Lodz region of Poland. *Pol J Pathol*. 60(2):76-80. PMID: 19886181.
10. Pierce, A. J., Johnson, R. D., Thompson, L. H., & Jasin, M. (1999). XRCC3 is required for efficient repair of chromosome breaks by homologous recombination. *Molecular Cell*, 4(2), 357–365.
11. Zhiyong Mao, Ying Jiang, Xiang Liu, Andrei Seluanov, Vera Gorbunova, DNA Repair by Homologous Recombination, But Not by Nonhomologous End Joining, Is Elevated in Breast Cancer Cells, *Neoplasia*, Volume 11, Issue 7, 2009, Pages 683-693, ISSN 1476-5586, <https://doi.org/10.1593/neo.09312>.
12. Griffin, C. S., Simpson, P. J., Wilson, C. R., & Thacker, J. (2000). Mammalian recombination-repair genes XRCC2 and XRCC3 promote correct chromosome segregation. *Nature Cell Biology*, 2(10), 757–761. https://www.nature.com/articles/ncb1000_757
13. Lucena-Cacace, A., Robles-Fernández, I., Carrasco-García, E., & Menéndez-Gutiérrez, M. P. (2016). Targeting DNA double-strand break repair for cancer therapy. *Cellular and Molecular Life Sciences*, 73(16), 2879–2894
14. Lieber, M. R. (2010). The mechanism of double-strand DNA break repair by the nonhomologous DNA end-joining pathway. *Annual Review of Biochemistry*, 79, 181–211. <https://doi.org/10.1146/annurev.biochem.052308.093131>
15. Scully, R., Panday, A., Elango, R., & Willis, N. A. (2019). DNA double-strand break repair-pathway choice in somatic mammalian cells. *Nature Reviews Molecular Cell Biology*, 20(11), 698–714. <https://doi.org/10.1038/s41580-019-0152-0>
16. Ergen, A., Cark, A., & Tuna, B. (2022). Association of XRCC3, XRCC4, BAX, and BCL-2 polymorphisms with the risk of breast cancer. *International Journal of Breast Cancer*, 2022, 2827649.
17. Kailas D. Datkhilea, Rashmi A. Gudur , Suresh J. Bhosale, Pratik P. Durgawale, Nilam J. Jagdale, Ashwini L. More, Anand K. Gudur , Satish R. Patil. (2023). Impact of Interaction between Single Nucleotide Polymorphism of XRCC1, XRCC2, XRCC3 with Tumor Suppressor TP53 Gene Increases Risk of Breast Cancer: A Hospital-Based Case-Control Study “(2023). *Asian Pacific Journal of Cancer Prevention*, 24(9), 3065–3075.
18. Liu, N., Lamerdin, J. E., Tebbs, R. S., Schild, D., et al. (1998). XRCC2 and XRCC3, new human Rad51-family members, promote chromosome stability and protect against DNA cross-links and other damages. *Molecular and Cellular Biology*, 18(10), 6146–6153. <https://doi.org/10.1128/MCB.18.10.6146>
19. Pelttari, L. M., Kiiski, J. I., Nurminen, R., et al. (2015). A recurrent mutation in XRCC3 observed in Finnish breast cancer patients. *Springer Plus*, 4, 88. <https://doi.org/10.1186/s40064-015-0880-3>
20. Ramatenki V, Potlapally SR, Dumpati RK, Vadija R, Vuruputuri U. Homology modeling and virtual screening of ubiquitin conjugation enzyme E2a for designing a novel selective antagonist against cancer. *J Recept Signal Transduct Res*. 2015;35(6):536-49. doi: 10.3109/10799893.2014.969375. Epub 2015 Sep 4. PMID: 25316404
21. The UniProt Consortium. (2023). UniProt: the Universal Protein Knowledgebase in 2023. *Nucleic Acids Research*, 51(D1), D523–D531. <https://doi.org/10.1093/nar/gkac1052>
22. Drozdetskiy, A., Cole, C., Procter, J., & Barton, G. J. (2015). JPred4: a protein secondary structure prediction server. *Nucleic Acids Research*, 43(W1), W389–W394. <https://doi.org/10.1093/nar/gkv332>
23. Kelley, L. A., et al. (2015). The Phyre2 web portal for protein modeling. *Nature Protocols*, 10(6), 845–858. <https://doi.org/10.1038/nprot.2015.053>
24. Thompson, J. D., et al. (1994). CLUSTAL W: improving the sensitivity of progressive multiple sequence alignment. *Nucleic Acids Res*, 22(22), 4673–4680.
25. Webb, B., & Sali, A. (2016). Comparative protein structure modeling using MODELLER. *Current Protocols in Bioinformatics*, 54(1), 5.6.1–5.6.37. <https://doi.org/10.1002/cpbi.3>
26. Friesner, R. A., Banks, J. L., Murphy, R. B., Halgren, T. A., et al. (2004). Glide: A new approach for rapid, accurate docking and scoring. 1. Method and assessment of docking accuracy. *Journal of Medicinal Chemistry*, 47(7), 1739–1749. <https://doi.org/10.1021/jm0306430>

27. Laskowski, R. A., MacArthur, M. W., Moss, D. S., & Thornton, J. M. (1993). PROCHECK: A program to check the stereochemical quality of protein structures. *Journal of Applied Crystallography*, 26(2), 283–291. <https://doi.org/10.1107/S0021889892009944>
28. Wiederstein M & Sippl MJ (2007) ProSA-web: interactive web service for the recognition of errors in three-dimensional structures of proteins. *Nucleic Acids Res* 35, W407–W410
29. Lüthy, R., Bowie, J. U., & Eisenberg, D. (1992). Assessment of protein models with three-dimensional profiles. *Nature*, 356(6364), 83–85. <https://doi.org/10.1038/356083a0>
30. Tian, W., et al. (2018). CASTp 3.0: computed atlas of surface topography of proteins. *Nucleic Acids Res*, 46(W1), W363–W367. <https://doi.org/10.1093/nar/gky473>
31. Halgren, T. A. (2009). Identifying and characterizing binding sites and assessing drug ability. *Journal of Chemical Information and Modeling*, 49(2), 377–389. <https://doi.org/10.1021/ci800324m>
32. Sastry, G. M., Adzhigirey, M., Day, T., Annabhimoju, R., & Sherman, W. (2013). Protein and ligand preparation: Parameters, protocols, and influence on virtual screening enrichments. *Journal of Computer-Aided Molecular Design*, 27(3), 221–234.
33. R Dumpati, V Ramatenki, R Vadija, S Vellanki, U Vuruputuri. (2018). Structural insights into suppressor of cytokine signaling 1 protein-identification of new leads for type 2 diabetes mellitus, *Journal of Molecular Recognition* 31 (7), e2706
34. R Dumpati, R Dulapalli, B Kondagari, V Ramatenki, S Vellanki, R Vadija. (2016). Suppressor of cytokine signalling-3 as a drug target for type 2 diabetes mellitus: a structure-guided approach, *Chemistry Select* 1 (10), 2502-2514
35. Muddagoni et al. (2021): Homology modeling validated with ProSA and Verify3D; binding-site identification via SiteMap; virtual screening using Schrödinger suite (LigPrep → Glide docking → QikProp ADME profiling). doi: 10.3389/fphar.2024.1387629. PMID: 38846093; PMCID: PMC11153788.
36. Banerjee, P., et al. (2018). ProTox-II: prediction of toxicity of chemicals. *Nucleic Acids Res*, 46(W1), W257–W263. <https://doi.org/10.1093/nar/gky318>
37. Drwal, M. N., Banerjee, P., Dunkel, M., Wettig, M. R., & Preissner, R. (2014). ProTox: a web server for the in silico prediction of rodent oral toxicity. *Nucleic Acids Research*, 42(W1), W53–W58.
38. Gebrehiwot H, Ensermu U, Dekebo A, Endale M, Nefo Duke T. (2024). *In Vitro* Antibacterial and Antioxidant Activities, Pharmacokinetics, and *In Silico* Molecular Docking Study of Phytochemicals from the Roots of *Ziziphus spina-christi*. *Biochem Res Int*. 9;2024:7551813. doi: 10.1155/2024/7551813. PMID: 39263680; PMCID: PMC11390196.
39. Laskowski, R. A., MacArthur, M. W., Moss, D. S., & Thornton, J. M. (1993). PROCHECK: A program to check the stereochemical quality of protein structures. *Journal of Applied Crystallography*, 26(2), 283–291. <https://doi.org/10.1107/S0021889892009944>
40. Bhargavi, M., & Bhargavi, S. G. (2025). Computational approach for HDAC1 predicting protein–ligand interactions for cancer through homology modelling, virtual screening and molecular docking. *Shanlax Publications – Computational Technology & Biology*. <https://www.shanlaxpublications.com/p/ctbtl/ch002.pdf>
41. Pavan, D. V., & Shankar, R. (2025). To evaluate the structural mechanism of M2-1 protein in the human respiratory syncytial virus using molecular docking software. *AIP Conference Proceedings*, 3270(1), 020175. <https://pubs.aip.org/aip/acp/article-abstract/3270/1/020175/3343834>
42. Laskowski, R. A. (2001). PDBsum: summaries and analyses of PDB structures. *Nucleic Acids Research*, 29(1), 221–222. <https://doi.org/10.1093/nar/29.1.221>
43. Laskowski, R. A., Jabłońska, J., Pravda, L., Vařeková, R. S., & Thornton, J. M. (2018). PDBsum: Structural summaries of PDB entries. *Protein Science*, 27(1), 129–134. <https://doi.org/10.1002/pro.3289>
44. Lyu C, Chen T, Qiang B, Liu N, Wang H, Zhang L, Liu Z. (2021). CMNPD: a comprehensive marine natural products database towards facilitating drug discovery from the ocean. *Nucleic Acids Res*. 8;49(D1):D509–D515. doi: 10.1093/nar/gkaa763. PMID: 32986829; PMCID: PMC7779072.
45. Afendi, F. M., Okada, T., Yamazaki, M., Hirai-Morita, A., Nakamura, Y., Nakamura, K., ... & Saito, K. (2020). CMNPD: A comprehensive marine natural products database towards facilitating drug discovery from the ocean. *Nucleic Acids Research*, 48(D1), D509–D516. <https://doi.org/10.1093/nar/gkz890>
46. Bhat, B. A., Algaissi, A., Khamjan, N. A., Dar, T. U. H., & Qasir, N. (2024). Exploration of CMNPD against Dengue viral NS1 protein using high-throughput computational studies. *Journal of Biomolecular Structure and Dynamics*. <https://doi.org/10.1080/07391102.2023.2297006>
47. BIOVIA, Dassault Systèmes. (2020). *Discovery Studio Modeling Environment*, Release 2020. San Diego, CA:
48. Lipinski, C. A., Lombardo, F., Dominy, B. W., & Feeney, P. J. (2001). Experimental and computational approaches to estimate solubility and permeability in drug discovery and development settings. *Advanced Drug Delivery Reviews*, 46(1–3), 3–26. [https://doi.org/10.1016/S0169-409X\(00\)00129-0](https://doi.org/10.1016/S0169-409X(00)00129-0)
49. Congreve, M., Carr, R., Murray, C., & Jhoti, H. (2003). A ‘rule of three’ for fragment-based lead discovery? *Drug Discovery Today*, 8(19), 876–877. [https://doi.org/10.1016/S1359-6446\(03\)02831-9](https://doi.org/10.1016/S1359-6446(03)02831-9)

Copyright: © 2025 Author. This is an open access article distributed under the Creative Commons Attribution License, which permits unrestricted use, distribution, and reproduction in any medium, provided the original work is properly cited.